Journal of Computational Physics 227 (2008) 8753–8767

Contents lists available at ScienceDirect

Journal of Computational Physics

journal homepage: www.elsevier.com/locate/jcp

Stable and accurate wave-propagation in discontinuous media

Ken Mattsson *, Frank Ham, Gianluca Iaccarino

Department of Information Technology, Uppsala University, MIC, Polacksbacken, 751 05 Uppsala, Sweden

ARTICLE INFO

Article history:
Received 22 March 2007
Received in revised form 11 January 2008
Accepted 20 June 2008
Available online 2 July 2008

Keywords:
High-order finite difference methods
Unstructured finite volume method
Wave equation
Numerical stability
Second derivatives
Discontinuous media
Complex geometries

ABSTRACT

A time stable discretization is derived for the second-order wave equation with discontinuous coefficients. The discontinuity corresponds to inhomogeneity in the underlying medium and is treated by splitting the domain. Each (homogeneous) sub domain is discretized using narrow-diagonal summation by parts operators and, then, patched to its neighbors by using a penalty method, leading to fully explicit time integration. This discretization yields a time stable and efficient scheme. The analysis is verified by numerical simulations in one-dimension using high-order finite difference discretizations, and in three-dimensions using an unstructured finite volume discretization.

1. Introduction

In many applications, such as general relativity [33,3], seismology [15,36], oceanography [27], acoustics [35,30,7,1,8] and electromagnetics [37,9], the underlying equations are systems of second-order hyperbolic partial differential equations. However, as pointed out in [18], with very few exceptions the equations are rewritten and solved as a system of first-order equations. There are three obvious drawbacks with this approach: (1) the number of unknowns is doubled, (2) spurious oscillations due to unresolved features might be introduced, and (3) double resolution (both in time and in each of the spatial dimensions) is required to obtain the same accuracy. The reasons for solving the equations on first-order form are most likely related to the maturity of CFD, that has evolved during the last 40 years. Many of the stability issues for first-order hyperbolic problems have already been addressed.

For wave-propagation problems, the computational domain is often large compared to the wavelengths, which means that waves have to travel long distances (or correspondingly long times). It can be shown that high-order accurate time marching methods, as well as high-order spatially accurate schemes (at least third-order) are more efficient [21] for problems on smooth domains. Such schemes, although they might be G–K–S stable [10] (convergence to the true solution as $\Delta x \to 0$), may exhibit a non-physical growth in time [4], for realistic mesh sizes. It is therefore important to devise schemes that do not allow a growth in time that is not called for by the differential equation. Such schemes are called strictly (or time) stable.

High-order accurate finite difference methods (HOFDM) are widely used for hyperbolic problems written on first-order form. For problems with discontinuous coefficients, the formal order of accuracy reduces to first-order [11,12,2] with no special treatment of the discontinuity. In this paper we will focus the attention to second-order formulations of the acoustic

* Corresponding author. Tel.: +46 18 4717631; fax: +46 18 523049.
E-mail address: ken.mattsson@it.uu.se (K. Mattsson).

0021-9991/$ - see front matter © 2008 Elsevier Inc. All rights reserved.
doi:10.1016/j.jcp.2008.06.023

wave equation in discontinuous media. One of the main motivations with this paper is to present a method that will recover high-order accuracy in the presence of discontinuous coefficients.

Traditionally, there have been essentially two approaches of handling the discontinuity, sometimes referred to as the heterogeneous and the homogeneous formulations [15]. In the heterogeneous approach [35,30,7], the discontinuity (here denoted *discontinuous interface*) is treated by taking an average "smoothing" of the spatially varying coefficients to recover stability. The benefit with this technique is that irregular shaped discontinuous interfaces are handled with no special treatment. However, the formal order of accuracy reduces to first-order.

The second approach to handle the discontinuity is to employ a domain decomposition technique and solve for the interface (jump) conditions. There are different techniques of imposing the interface conditions. In [1] a second-order FD method is introduced where the solution is based on the introduction of auxiliary Lagrange multipliers. A drawback with this technique is that a huge system of linear equations has to be solved at each time-step. It is unclear if this technique can be extended to handle irregular shaped discontinuous interfaces, and how to obtain higher-order accuracy. A strictly stable HODFM for the wave equations in discontinuous media was constructed in [24] by combining second-derivative summation-by-parts (SBP) operators (constructed in [23]) with the projection method [28,29] to impose the boundary and the discontinuous interface (jump) conditions. The drawback with this approach is that it cannot easily be extended to handle variable coefficients (except pice-wise constant coefficients), complex geometries and irregular shaped discontinuous interfaces. In [18,19,17,16] a second-order accurate FD method for the acoustic wave equation on second-order form is constructed, where the discontinuity and complex geometry are handled by embedding the domain into a Cartesian grid, making use of ghost-points and Lagrange interpolation to impose the boundary and interface conditions. It is unclear if the embedded boundary method can be extended to higher-order accuracy. Another good candidate is the discontinuous Galerkin (DG) method, which combines both unstructured capability and higher-order accuracy (also in discontinuous media). DG have been implemented successfully in 2-D for both the acoustic wave equation [8] and Maxwell's equations [9] on second-order form. However, the efficiency of DG applied to systems of second-order hyperbolic equations on large 3-D applications is an open question.

In this paper we focus on: (1) deriving strictly stable HOFDM for the acoustic wave equation in discontinuous media, by combining second-derivative SBP operators and the simultaneous approximation term (SAT) method [5], and (2) introducing the technique in complex geometries by making use of the discrete Laplacian operator used in CDP[1] (an unstructured finite volume flow solver developed as part of Stanford's DOE-funded ASC Alliance program to perform LES in complex geometries). This approach is somewhat related to the DG method since they both make use of the penalty technique to handle the discontinuity in a truly non-overlap fashion.

The three reasons for introducing the SAT method instead of the recently developed projection method [24] to impose the discontinuous interface conditions are the following: (1) it is easier to implement (although, a detailed study is omitted here), (2) it is not limited to piecewise constant coefficients (see [24]), and (3) it is much more accurate (as will be shown in Section 4).

The two main reasons for introducing computational tools from CDP are the following: (1) it allows us to handle huge problems in complex geometries, and (2) it makes it easier to isolate and verify the accuracy and stability properties of the Laplacian operator used in CDP. (In spite of it's simplicity the second-order wave equation imposes a stricter stability requirement [24] on the discrete Laplacian operator than when used for parabolic problems like the Navier–Stokes equations).

In Section 2 we introduce some definitions and discuss the SBP property for the 1-D case, and show how to impose the boundary and interface conditions in discontinuous media using SAT. In Section 3 we will show how to implement this technique in complex geometries using the unstructured finite volume method. In Section 4 we will verify the accuracy and stability properties, by performing numerical computations in 1-D and 3-D. A direct comparison between the SAT method and the Projection method will be done for the 1-D case. In Section 5 we present our conclusions.

In this article, we only consider acoustic waves. The extension to handle for example elastic waves [15,2,36] with an analogous approach will be dealt with in a forthcoming paper.

2. The finite difference method

For clarity we will restrict the analysis to 1-D in this section. The extension to 2-D and 3-D (see for example [24,26,25]) is straightforward using 1-D SBP finite-difference operators.

We begin with a short description and some definitions (for more details, see [20,31,23]). Let the inner product for real-valued functions $u, v \in L^2[-1,1]$ be defined by $(u,v) = \int_{-1}^{1} u\, v\, w\, dx$, $w(x) > 0$, and let the corresponding norm be $\|u\|_w^2 = (u,u)$. The domain $(-1 \leqslant x \leqslant 1)$ is discretized using $2N+1$ equidistant grid points

$$x_i = i\,h, \quad i = 0, 1 \ldots, 2N, \quad h = \frac{2}{N}.$$

[1] CDP is named after Charles David Pierce (1969–2002).

The approximative solution at grid point x_i is denoted v_i, and the discrete solution vector is $v^{\mathrm{T}} = [v_0, v_1, \ldots, v_{2N}]$. Similarly, we define an inner product for discrete real-valued vector functions $u, v \in \mathbf{R}^{2N+1}$ by $(u, v)_H = u^{\mathrm{T}} H v$, where $H = H^{\mathrm{T}} > 0$, with the corresponding norm $\|v\|_H^2 = v^{\mathrm{T}} H v$. The following vectors will be frequently used:

$$e_0 = [1, 0, \ldots, 0]^{\mathrm{T}}, \quad e_N = [0, \ldots, 0, 1]^{\mathrm{T}}. \tag{1}$$

2.1. Narrow-diagonal SBP operators

To introduce narrow-diagonal SBP operators, we present the following definition:

Definition 2.1. An explicit pth-order accurate finite difference scheme with minimal stencil width of a Cauchy problem, is called a pth-order accurate narrow stencil.

Remark. We say that a scheme is explicit if no linear system of equations need to be solved to compute the difference approximation. Spatial Padé discretizations [22] are often referred to as "compact schemes". The approximation of the derivative is obtained by solving a tri- or penta-diagonal system of linear equations at every time-step. Hence, if written in explicit form, Padé discretizations lead to full-difference stencils, similar to spectral discretizations.

Consider the 1-D wave equation

$$a u_{tt} = (b u_x)_x \quad x \in [-1, 1], \tag{2}$$

where $a(x), b(x) > 0$. Multiplying Eq. (2) by u_t and integrating by parts (referred to as "the energy method") lead to

$$\frac{\mathrm{d}}{\mathrm{d}t} E = 2 b u_t u_x|_{-1}^{1}, \tag{3}$$

where the continuous energy is defined as

$$E = (\|u_t\|_a^2 + \|u_x\|_b^2). \tag{4}$$

Definition 2.2. Let $D_2^{(b)} = H^{-1}(-M_b + BS)$ approximate $\partial/\partial x(b\partial/\partial\, x)$, where $b(x) > 0$ is a smooth function, using a pth-order accurate narrow stencil. $D_2^{(b)}$ is said to be a pth-order accurate narrow-diagonal second-derivative SBP operator, if H is diagonal and positive definite, M_b is symmetric and positive semi-definite, S approximates the first-derivative operator at the boundaries and $B = \mathrm{diag}(-b_0, 0 \ldots, 0, b_N)$.

A second-order accurate narrow-diagonal second-derivative SBP operator $D_2^{(b)}$ is presented in Appendix I. (High-order accurate narrow-diagonal second-derivative SBP operators for constant coefficients $b(x) = 1$, denoted D_2, were constructed in [23]. For completeness we present the second-, fourth-, and sixth-order accurate operators in Appendix I, since they are used in Section 4.) An example of its use is the semi-discretization $A v_{tt} = D_2^{(b)} v$ of (2), where A is the projection of a onto the diagonal. Multiplying by $v_t^{\mathrm{T}} H$ from the left and adding the transpose lead to

$$\frac{\mathrm{d}}{\mathrm{d}t} E_H = 2(v_t)_0 (BSv)_0 + 2(v_t)_N (BSv)_{2N}, \tag{5}$$

where the semi-discrete energy is defined as

$$E_H = (\|v_t\|_{HA}^2 + v^{\mathrm{T}} M_b v). \tag{6}$$

Estimate (5) is a discrete analog of Eq. (3).

Remark. The discrete energy (6) mimics Eq. (4) iff: (1) H is diagonal and positive definite, and (2) if M_b is positive-definite and the interior stencil is a narrow approximation of $-h\partial/\partial x(b\partial/\partial x)$. The first condition guarantees that the matrix product HA is a norm (i.e., symmetric and positive definite). The second condition guarantees that $v^{\mathrm{T}} M_b v \geqslant 0$ with equality iff v is a constant (such that the quadratic form exactly mimics $\|u_x\|_b$). If M_b is not narrow $v^{\mathrm{T}} M_b v$ is zero also for v equal to the highest frequency mode that can exist on the grid (sometimes referred to as spurious oscillations), which means that stability is not guaranteed.

The following lemma is central to the present study:

Lemma 2.3. *The dissipative part M_b of a narrow-diagonal second-derivative SBP operator has the following property:*

$$v^{\mathrm{T}} M_b v = h\ \frac{\alpha}{b_0} (BSv)_0^2 + h\ \frac{\alpha}{b_N} (BSv)_N^2 + v^{\mathrm{T}} \widetilde{M}_b v, \tag{7}$$

where $\widetilde{M}_b$ is symmetric and positive semi-definite, and α a positive constant, independent of h.

Table 1
α in Eq. (7) for the second-, fourth- and sixth-order accurate narrow-diagonal second-derivative SBP operators

Second-order	Fourth-order	Sixth-order
1	0.2508560249	0.1878715026

Proof. See Appendix I. □

This was indicated in [6] but never derived explicitly. For the special but important case of constant coefficients ($b = 1$) we have derived numerically the values of α for the second-, fourth- and sixth-order accurate finite difference SBP discretizations (see Appendix I) by using the symbolic mathematics software Maple. The results are presented in Table 1.

Remark. The boundary closure for a pth-order accurate narrow-diagonal SBP operator is of order $p/2$ (see [23]). This means that the boundary closure for $(D_1)^2$ is of order $p/2 - 1$. Hence, for second-order hyperbolic systems the convergence for wide-stencil approximations (i.e., by replacing D_2 with $(D_1)^2$) drops to $(p/2+1)$th-order, while the narrow-stencil formulations are $(p/2+2)$th-order accurate (see [32] for more information on the accuracy of finite difference approximations).

2.2. Media interface in 1-D

We start by deriving the interface conditions for the continuous problem (2), where the coefficients $a(x), b(x) > 0$ are discontinuous at $x = 0$. Integration by parts leads to

$$\begin{aligned}\int_{-1}^{1} a u_{tt} u_t \, dx &= \lim_{\epsilon \to 0} \left(\int_{-1}^{-\epsilon} (b \, u_x)_x u_t \, dx - \int_{1}^{\epsilon} (b \, u_x)_x u_t \, dx \right) \\ &= \lim_{\epsilon \to 0} \left(b \, u_x u_t |_{-1}^{1} - b \, u_x u_t |_{-\epsilon}^{\epsilon} - \int_{-1}^{-\epsilon} b \, u_x u_{xt} \, dx + \int_{1}^{\epsilon} b \, u_x u_{xt} \, dx \right).\end{aligned}$$

To obtain an energy estimate requires that u_t and $b u_x$ are continuous across the interface, i.e., $\lim_{\epsilon \to 0} (b \, u_x u_t |_{-\epsilon}^{\epsilon}) = 0$, leading to Eq. (3). We consider the following problem:

$$\begin{aligned} a_1 u_{tt}^{(1)} &= (b_1 u_x^{(1)})_x, \quad -1 \leqslant x \leqslant 0 \\ a_2 u_{tt}^{(2)} &= (b_2 u_x^{(2)})_x, \quad 0 \leqslant x \leqslant 1, \end{aligned} \tag{8}$$

where $a_1 \neq a_2$, $b_1 \neq b_2$. Here $u^{(1,\,2)}$ denote the solutions corresponding to the left and right domains respectively. Continuity at the interface ($x = 0$) means that the following interface (jump) conditions:

$$u_t^{(1)} = u_t^{(2)}, \quad b_1 u_x^{(1)} = b_2 u_x^{(2)} \tag{9}$$

have to be imposed. (The first interface condition in Eq. (9) holds if we impose $u^{(1)} = u^{(2)}$ at the interface. This will have implications when we turn to the numerical treatment, in particular the time-discretization, see the remark at the end of this section.) At the far-field boundaries we apply Neumann boundary conditions

$$\begin{aligned} -b_1(-1) u_x^{(1)}(-1, t) &= g_{-1}(t) \\ b_2(1) u_x^{(2)}(1, t) &= g_1(t). \end{aligned} \tag{10}$$

Remark. Other type of boundary conditions, like Dirichlet and radiation boundary conditions (see for example [34,13]) can also be used. However, the main focus in this paper is on the interface treatment.

To simplify the coming energy-estimates we will always assume homogeneous boundary data. (The analysis holds for inhomogeneous data, but introduces unnecessary notation.)

The energy method applied to Eq. (8) with the interface conditions (9) and the homogeneous Neumann boundary conditions (10) leads to

$$\frac{d}{dt} E^{(2)} = 0, \tag{11}$$

where the energy is defined as

$$E^{(2)} = \|u_t\|_{a_1}^2 + \|v_t\|_{a_2}^2 + \|u_x\|_{b_1}^2 + \|v_x\|_{b_2}^2. \tag{12}$$

We introduce $E^{(2)}$ to denote the fact that Eq. (8) consists of two sub domains.

The semi-discrete approximation of (9) can be written

$$\begin{aligned} I_1 &\equiv v_N^{(1)} - v_0^{(2)} = 0 \quad I_2 \equiv (v_t^{(1)})_N - (v_t^{(2)})_0 = 0 \\ I_3 &\equiv (B_1 S v^{(1)})_N + (B_2 S v^{(2)})_0 = 0, \end{aligned} \tag{13}$$

where all conditions (also $v_N^{(1)} = v_0^{(2)}$) are written out. Here $v^{(1,2)}$ are the solution vectors corresponding to the left and right domains respectively. The left and right domains are discretized using $(N+1)$ grid points.

A semi-discretization of (10) is given by

$$L_1^{\mathrm{T}} v^{(1)} = (BSv^{(1)})_N^{(1)} = g_{-1}, \quad L_2^{\mathrm{T}} v^{(2)} = (BSv^{(2)})_0 = g_1. \tag{14}$$

The reason why we write out $g_{1,-1}$ (although we will set $g_{1,-1} = 0$ in the coming energy estimate) is to emphasize the nature of SAT (as a penalty forcing function) and to show the more general case of time-dependent data. A semi-discretization of Eq. (8) using narrow-diagonal SBP operators and the SAT method to impose the semi-discrete interface conditions (13) and boundary conditions (14), can be written:

$$\begin{aligned} A_1 v_{tt}^{(1)} &= D_2^{(b_1)} v^{(1)} & A_2 v_{tt} &= D_2^{(b_2)} v^{(2)} \\ &\quad +\tau H^{-1} e_N(I_1) & &\quad -\tau H^{-1} e_0(I_1) \\ &\quad +\beta (BS)^{\mathrm{T}} e_N H^{-1}(I_1) & &\quad -\beta (BS)^{\mathrm{T}} e_0 H^{-1}(I_1) \\ &\quad +\gamma H^{-1} e_N(I_3) & &\quad -\gamma H^{-1} e_0(I_3) \\ &\quad +\sigma H^{-1} e_N(I_2) & &\quad -\sigma H^{-1} e_0(I_2) \\ &\quad -H^{-1} e_0(L_1^{\mathrm{T}} v^{(1)} - g_{-1}) & &\quad +H^{-1} e_N(L_2^{\mathrm{T}} v^{(2)} - g_1). \end{aligned} \tag{15}$$

The first main result of this paper is stated in the following Lemma:

Lemma 2.4. *The scheme (15) with homogeneous data is stable if $D_2^{(b_{1,2})}$ are narrow-diagonal SBP operators, $\sigma \leqslant 0$, $\gamma = -\frac{1}{2}$, $\beta = \frac{1}{2}$ and $\tau \leqslant -\frac{b_1+b_2}{4h\alpha}$ hold.*

Proof. Let $g_{-1} = g_1 = 0$, and $\gamma = \frac{1}{2}$, $\beta = -\frac{1}{2}$. Multiplying Eq. (15) by $(v^{(1)})_t^{\mathrm{T}} H$ and $(v_t^{(2)})^{\mathrm{T}} H$, respectively, and adding the transpose lead to

$$\frac{\mathrm{d}}{\mathrm{d}t} E_H^{(2)} = 2\, w_t^{\mathrm{T}} D w_t + \frac{\mathrm{d}}{\mathrm{d}t} x^{\mathrm{T}} R x,$$

where the right hand side corresponds to the interface coupling terms given by

$$w = \begin{bmatrix} v_N^{(1)} \\ v_0^{(2)} \end{bmatrix}, \quad D = \sigma \begin{bmatrix} 1 & -1 \\ -1 & 1 \end{bmatrix},$$

and

$$x = \begin{bmatrix} v_N^{(1)} \\ v_0^{(2)} \\ (BSv^{(1)})_N \\ (BSv^{(2)})_0 \end{bmatrix}, \quad R = \begin{bmatrix} -\tau & \tau & -\frac{1}{2} & \frac{1}{2} \\ \tau & -\tau & -\frac{1}{2} & \frac{1}{2} \\ -\frac{1}{2} & -\frac{1}{2} & -\frac{\alpha}{b_1} & 0 \\ \frac{1}{2} & \frac{1}{2} & 0 & -\frac{\alpha}{b_2} \end{bmatrix}.$$

Here we have used Lemma 2.3 and the fact that $D_2^{(b_1,b_2)}$ are narrow-diagonal SBP operators. The discrete energy is given by

$$E_H^{(2)} = \|v_t^{(1)}\|_{HA_1}^2 + \|v_t^{(2)}\|_{HA_2}^2 + (v^{(1)})^{\mathrm{T}} M_{b_1} v^{(1)} + (v^{(2)})^{\mathrm{T}} M_{b_2} v^{(2)}.$$

Stability follows if D and R are negative semi-definite, which lead to the following conditions:

$$\sigma \leqslant 0 \quad , \tau \leqslant -\frac{b_1+b_2}{4h\alpha},$$

where $b_{1,2}$ denote the local values of $b_{1,2}$ at the interface. □

Remark. By choosing $\sigma = 0$ in (15) a compact (only two time-levels have to be stored) and explicit high-order accurate time-discretization can be used (see [24] for details). This is the choice in the computations. If $\sigma < 0$ damping of the energy is introduced, which can potentially lead to a more robust and less reflective interface treatment. For this case the standard fourth-order accurate Runge–Kutta method can be used to time-advance the solution. We have not included a numerical study for the case where $\sigma < 0$ in this paper.

We introduce the penalty-strength parameter Γ through

$$\tau = -\Gamma \frac{b_1+b_2}{4h\alpha}.$$

Hence a value of $\Gamma < 1$, according to Lemma 2.4, will not result in an energy estimate and might lead to an unstable scheme. A higher value of Γ leads to a more tight interface coupling. This can potentially lead to a more accurate coupling, but will also introduce stiffness. This is verified numerically in Section 4.

3. The finite volume method

This section describes the details of the discrete Laplacian finite volume operator used to develop the internal discretization and boundary conditions in CDP. The operator is developed for a node-based discretization on general polyhedral meshes, where both grid coordinates and the unknowns are collocated at nodes. Fig. 1 provides some geometrical details used for operator construction. The discretization of the Laplacian operator is particularly challenging for unstructured finite volume methods because it is difficult to simultaneously achieve accuracy and stability on general unstructured grids. Consider the 3-D wave equation

$$au_{tt} = b\ \Delta u, \tag{16}$$

where $b,\ a(x,y,z) > 0$. To simplify notation in this section we assume that b is constant (compare with Eq. (2) in 1-D), although CDP can handle variable coefficients.

To introduce the narrow-diagonal Laplacian operator (compare with Definition 2.2 in the 1-D case.), we present the following two definitions:

Definition 3.1. Let $S = \sum_{i\in F_b'} S_{i,b}$, where F_b' is the set of all boundary sub-faces. $S_{i,b}$ is an outward sub-face normal derivative operator associated with each of the boundary nodes. We say that S approximates the outward normal derivative operator at the boundary.

Definition 3.2. Let $D_L = V^{-1}(-L+S)$ approximate the Laplacian operator. D_L is said to be a narrow-diagonal Laplacian SBP operator, if V is diagonal and positive definite, L is narrow, symmetric and positive semi-definite, and S as defined in Definition 3.1.

A semi-discretization of (16), using a narrow-diagonal Laplacian SBP operator, will have the following matrix form:

$$VAv_{tt} = b(-L+S)v. \tag{17}$$

We will now describe the construction of the narrow-diagonal Laplacian SBP operator on an unstructured 3-D mesh. In Section 4 we will use this operator to simulate wave-propagation in complex discontinuous media in 3-D.

3.1. Narrow-diagonal Laplacian SBP operator

The node-based volumes required for integrating the time derivative and any source terms are computed by tessellating each cell into "sub-tets", each defined by a node, an edge, a face, and a cell as shown in Fig. 1. The volume of the sub-tet is then added to the volume associated with node P. In the current version of CDP, the volume or mass matrix is thus diagonal (lumped-mass approximation). Row P of the volume integration operator V has a single diagonal entry equal to the sum of its associated sub-tet volumes $V_{t'}$:

$$V_P\ \phi \approx \int_P \phi\ \mathrm{d}V = \sum_{t'\in T_P'} V_{t'}\phi_P,$$

where ϕ is a scalar function, t' represents a sub-tet, and T_P' the set of all sub-tets associated with node P.

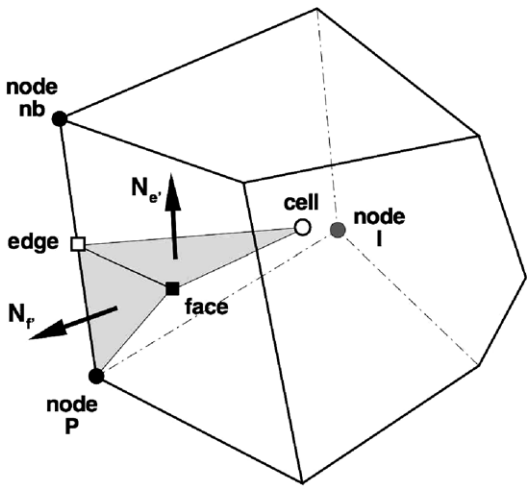

Fig. 1. Geometrical details for 3-D node-based meshes. Unknowns are stored at nodes (e.g., P and edge-based neighbor nb). Edge centers are located at the midpoint between nodes, face centers are located at the simple average of their surrounding nodes, and cell centers are defined by the simple average of their surrounding nodes. $N_{e'}$ is a sub-edge normal, associated with an internal or boundary edge. $N_{f'}$ is a sub-face normal associated with boundary faces only.

To further simplify the construction of these volumes and the operators in general, we choose the simple average of surrounding nodes to define face and cell centers. Unlike cell-centered control volume (CV) based formulations, where face and cell centers are defined at the centroids or centers of mass, the same definition for the node-based formulation has no obvious benefit. The choice of simple average for center locations ensures that interpolations based on simple averages of nodal data will be limited and linearly exact. For meshes built from simplex elements (pris/tets), the simple average is of course equivalent to the center of mass. In [14], we reported the results of a one-to-one comparison of the node-based and the CV-based formulations using the inviscid Taylor vortex problem on a variety of grids, and concluded that, with few exceptions, the nodal discretization was significantly more accurate, displaying consistent second-order rates of error reduction.

In CDP, the volume-integrated Laplacian operator is constructed using the divergence theorem and the sub-edge concept presented in Fig. 1. For row P of the narrow-diagonal Laplacian SBP operator

$$(-L_P + S_P)\ \phi \approx \int_P \frac{\partial^2 \phi}{\partial x_i \partial x_i} \mathrm{d}V = \oint_P \frac{\partial \phi}{\partial x_i} \hat{n}_i \ \mathrm{d}A = \sum_{e' \in E'_P} \left.\frac{\partial \phi}{\partial x_i}\right|_{e'} \hat{n}_{i,e'} A_{e'} + \sum_{f' \in F'_P} \left.\frac{\partial \phi}{\partial x_i}\right|_{f'} \hat{n}_{i,f'} A_{f'} = \sum_{e' \in E'_P} S_{e'} \phi + \sum_{f' \in F'_P} S_{f'} \phi,$$

where e' represents a sub-edge, E'_P the set of all sub-edges associated with node P, $f\prime$ represents a boundary sub-face, and F'_P the set of all boundary sub-faces associated with node P. $\hat{n}_{e'}$ is the sub-edge outward unit normal (outward with respect to P), $A_{e'}$ the sub-edge area, $S_{e'}$ and $S_{f'}$ are the sub-edge and sub-face normal-derivative-times-area operators, respectively. The required gradient for each sub-edge is determined by solving the following 3×3 system for the unknown gradient components:

$$\begin{aligned}
&\left.\frac{\partial \phi}{\partial x_i}\right|_{e'} (x_{i,nb} - x_{i,P}) = \phi_{nb} - \phi_P \\
&\left.\frac{\partial \phi}{\partial x_i}\right|_{e'} \left(\frac{1}{N_{nof}} \sum x_{i,nof} - \frac{1}{2}(x_{i,nb} + x_{i,P}) \right) = \frac{1}{N_{nof}} \sum \phi_{nof} - \frac{1}{2}(\phi_{nb} + \phi_P) \\
&\left.\frac{\partial \phi}{\partial x_i}\right|_{e'} \left(\frac{1}{N_{noc}} \sum x_{i,noc} - \frac{1}{2}(x_{i,nb} + x_{i,P}) \right) = \frac{1}{N_{noc}} \sum \phi_{noc} - \frac{1}{2}(\phi_{nb} + \phi_P),
\end{aligned}$$

where P and nb represent the two nodes associated with the edge of this sub-edge, *nof* the N_{nof} nodes of the face associated with the sub-edge (these will of course include P and nb) and *noc* the N_{noc} nodes of the cell associated with this sub-edge (these will also include P and nb).

It is important to note that the sub-edges are not combined into a single edge normal and edge area prior to dotting with an edge-based gradient. This combination of normals to a single edge normal may simplify the construction of the operator, but it is not done in CDP. As such, in addition to being compact and linearly exact (which, for a Laplacian, means returning zero in a linear field), the resulting operator has two important properties:

- In the limit of Cartesian structured meshes, the standard narrow-diagonal second-order finite difference Laplacian is recovered (involving only node P and the six neighbors that share an edge with P).
- For the case of simplex elements, the standard FEM Laplacian using linear basis functions is recovered.

The first of these properties is well known, and would have resulted even if we had combined the sub-edge normals into a single edge. The equivalence with linear FEM on simplex grids and resulting symmetry, however, is less well known and requires this sub-edge construction.

The boundary part of the Laplacian operator is a summation over sub-faces, and will be non-zero at boundary nodes only. The three required components of the gradient at each sub-face are determined by solving a similar 3×3 system, involving the two equations:

$$\begin{aligned}
&\left.\frac{\partial \phi}{\partial x_i}\right|_{f'} (x_{i,nb} - x_{i,P}) = \phi_{nb} - \phi_P \\
&\left.\frac{\partial \phi}{\partial x_i}\right|_{f'} \left(\frac{1}{N_{nof}} \sum x_{i,nof} - x_{i,P} \right) = \frac{1}{N_{nof}} \sum \phi_{nof} - \phi_P
\end{aligned}$$

and one of

$$\begin{aligned}
&\left.\frac{\partial \phi}{\partial x_i}\right|_{f'} (x_{i,I} - x_{i,P}) = \phi_I - \phi_P \\
&\left.\frac{\partial \phi}{\partial x_i}\right|_{f'} \left(\frac{1}{N_{noc}} \sum x_{i,noc} - x_{i,P} \right) = \frac{1}{N_{noc}} \sum \phi_{noc} - \phi_P,
\end{aligned}$$

with the first of these being preferred. Nodes P and nb are on the edge associated with the boundary sub-face, *nof* are the N_{nof} nodes of the face associated with the sub-face, I (for Internal) is/are the node(s) along the edge(s) of P not part of the boundary face, but still part of the internal cell that contains the boundary face, and *noc* are the N_{noc} nodes associated with the

internal cell that contains the boundary face. For clarity, node I is labeled in Fig. 1. Although the last equation is never used for grids composed of convex unstructured primitives (tet, pyramid, prism, hex), it is included here because on certain non-convex or polyhedral meshes (e.g., meshes with hanging nodes on boundary faces), the edges associated with node I can be coplanar with the boundary face.

While there are no restrictions on the complexity of $S_{f'}$ with regard to stability, here we have made the practical decision to define it in a way that simplifies the parallel implementation. In CDP the domain is decomposed such that the cells (elements) are uniquely divided among the processors. However, nodes, edges, and faces that lie on inter-processor boundaries are multiply defined. By expressing the $S_{f'}$ operator as a global sum of locally available information (the cell and boundary face that completely define the gradient are entirely present on only one processor). In addition, this local definition of $S_{f'}$ makes it straightforward to include only those sub-faces that participate in a particular interface or Neumann boundary condition.

Remark. Part of the stability requirement for the Laplacian SBP operator is that L is symmetric and positive semi-definite. For both the limiting cases previously described, it is well known that this is true. On general polyhedra, however, we do not have a proof. But an eigenvalue analysis (not shown here) using a variety of polyhedral meshes indicate that L is positive semi-definite except for the case of extreme element deformation.

The following lemma is central to the present study:

Lemma 3.3. *The dissipative part L of a narrow-diagonal Laplacian SBP operator has the following property:*

$$v^{\mathrm{T}} L v = \alpha \sum_{i \in F'_b} \frac{V_{i,b}}{A_{i,b}} (S_{i,b} v)^2 + v^{\mathrm{T}} \widetilde{L} v, \tag{18}$$

where F'_b is the set of all boundary sub-faces and $S_{i,b}$ as in Definition 3.1. $A_{i,b}$ is an area magnitude, and $V_{i,b}$ a nodal volume associated with each of the boundary nodes. $\widetilde{L}$ is symmetric and positive semi-definite and α a positive constant.

We omit the proof, since it is similar to the proof of Lemma 2.3. Unlike the uniform structured 1-D case, it is more complicated to analytically derive a single sharp value for α, that is applicable to all unstructured grids. A numerical eigenvalue analysis indicate that $\alpha \simeq 0.8$ for the problems computed in this article (compare with the second-order case in 1-D Table 1).

3.2. Media interface in 3-D

The 3-D extension of Eq. (8) (with the 1-D interface conditions (9) and Neumann boundary conditions (10)) is given by

$$\begin{aligned}
&a_1 u_{tt}^{(1)} = b_1\ \Delta u^{(1)}, \quad \mathbf{x} \in \Omega^{(1)} \\
&a_2 u_{tt}^{(2)} = b_2 \\
&Deltau^{(2)}, \quad \mathbf{x} \in \Omega^{(2)} \\
&b_1 \nabla u^{(1)} \cdot \mathbf{n}^{(1)} = g^{(1)}, \quad \mathbf{x} \in \partial\Omega^{(1)} \\
&b_2 \nabla u^{(2)} \cdot \mathbf{n}^{(2)} = g^{(2)}, \quad \mathbf{x} \in \partial\Omega^{(2)} \\
&b_1 \nabla u^{(1)} \cdot \mathbf{n}^{(1)} = -b_2 \nabla u^{(2)} \cdot \mathbf{n}^{(2)}, \quad \nabla u^{(1)} = u^{(2)}, \quad \nabla u_t^{(1)} = u_t^{(2)}, \quad \mathbf{x} \in \partial\Omega^{(I)},
\end{aligned} \tag{19}$$

where ∇ is the gradient operator and $\Omega^{(1,2)} \in \mathbf{R^3}$ are two adjacent domains (representing different media) joined by the interface $\partial\Omega^{(I)}$. $\partial\Omega^{(1,2)}$ are the boundaries of the adjacent domains, excluding $\partial\Omega^{(I)}$. $\mathbf{n}^{(1,2)}$ are the outward pointing normals corresponding to the two domains.

The semi-discrete finite volume approximation of (19) using narrow-diagonal Laplacian SBP operators and the SAT technique can be written:

$$\begin{aligned}
VA_1 v_{tt}^{(1)} &= b_1(-L+S)v^{(1)} \\
&\quad +\tau_{i,I} B_{i,I}^{(1)} (v^{(1)} - v^{(2)}) \\
&\quad +\beta S^{\mathrm{T}} B_{i,I}^{(1)} (v^{(1)} - v^{(2)}) \\
&\quad +\gamma B_{i,I}^{(1)} (b_1 S v^{(1)} + b_2 S v^{(2)}) \\
&\quad +\sigma B_{i,I}^{(1)} (v_t^{(1)} - v_t^{(2)}) \\
&\quad -B_{i,b}^{(1)} (b_1 S v^{(1)} - g^{(1)})
\end{aligned}
\qquad
\begin{aligned}
VA_2 v_{tt}^{(2)} &= b_2(-L+S)v^{(2)} \\
&\quad -\tau_{i,I} B_{i,I}^{(2)} (v^{(1)} - v^{(2)}) \\
&\quad -\beta S^{\mathrm{T}} B_{i,I}^{(2)} (v^{(1)} - v^{(2)}) \\
&\quad -\gamma B_{i,I}^{(2)} (b_1 S v^{(1)} + b_2 S v^{(2)}) \\
&\quad -\sigma B_{i,I}^{(2)} (v_t^{(1)} - v_t^{(2)}) \\
&\quad +B_{i,b}^{(2)} (b_2 S v^{(2)} - g^{(2)}),
\end{aligned} \tag{20}$$

where $B_{i,b}^{(1,2)}$ and $B_{i,I}^{(1,2)}$ picks out the outer boundary nodes (compare with Eq. (15)) and the interior interface nodes respectively, in the two domains (compare with $e_{0,N}$ in (1)). As for the 1-D case, $v^{(1,2)}$ denote the solution vectors corresponding to the two different domains (media).

The second main result of this paper is stated in the following Lemma:

Lemma 3.4. *The scheme (20) with homogeneous data is stable if $D_L = V^{-1}(-L+S)$ is a narrow-diagonal Laplacian SBP operator, $\sigma \leqslant 0$, $\gamma = -\frac{1}{2}$, $\beta = \frac{1}{2}$ and $\tau_{i,I} \leqslant -\frac{A_{i,b}}{V_{i,b}} \frac{b_1+b_2}{4\alpha}$ hold.*

We omit the proof, since it is similar to the proof of Lemma 2.4. (Note that $\tau_{i,I}$ varies along the interface depending on $A_{i,b}$ and $V_{i,b}$.)

4. Computations

To test the accuracy of Eqs. (15) and (20) we chose an analytic solution

$$\begin{aligned} u^{(1)} &= \cos(w_1 c_1 t)\ \cos(w_1 x), \quad x \in [-1,0], \quad t \geqslant 0, \quad w_1 = (2\ n+1)\pi, \quad m,n \in \mathbf{Z} \\ u^{(2)} &= \cos(w_2 c_2 t)\ \cos(w_2 x), \quad x \in [0,1], \quad t \geqslant 0, \quad w_2 = (2\ m+1)\pi, \quad c_2 = c_1 \frac{w_1}{w_2}, \end{aligned} \tag{21}$$

where $a_1 = b_1 = 1,\ a_2 = b_2 = 0.6$, $n = 1$ and $m = 2$ is used. (Here we have introduce the notation $c_k = a_k b_k$, $k = 1, 2$.)

The convergence rate is calculated as

$$q = \log_{10}\left(\frac{\|u - v^{(N_1)}\|_h}{\|u - v^{(N_2)}\|_h}\right) \Big/ \log_{10}\left(\frac{N_1}{N_2}\right)^{1/d}, \tag{22}$$

where d is the dimension ($d = 1$ in the 1-D case), $u = [u^{(1)}, u^{(2)}]$ is the analytic solution, and $v^{(N_1)}$ the corresponding numerical solution with N_1 unknowns. $\|u - v^{(N_1)}\|_h$ is the discrete l_2 norm of the error.

Eqs. (15) and (20) with $\sigma = 0$ and homogeneous data can formally be written as an ODE system

$$v_{tt} = Qv, \tag{23}$$

where $v^{\mathrm{T}} = [v^{(1)}, v^{(2)}]^{\mathrm{T}}$ is the discrete solution vector. In Sections 2 and 3 we have shown that the matrix Q have non-positive and real eigenvalues (a necessary stability condition) by utilizing the energy method. A compact (only two time-levels have to be stored) and explicit high-order accurate time-discretization is used (see [24]) for the time advancement. For a Cartesian grid it can be shown [24] that the time-step restriction (for stability) is inversely proportional to the square root of the spectral radius of Q.

Table 2
The spectral radius of $h^2 Q$ for Eq. (15) using different strength of penalty parameter Γ

Order	$\Gamma = 1$	$\Gamma = 1.2$	$\Gamma = 5$	Projection
Second	4.00	4.00	13.52	4.00
Fourth	5.77	6.33	31.60	5.32
Sixth	15.34	15.65	48.43	10.34

Also comparing to the projection method.

Table 3
$\log(l_2 - \text{error})$ and convergence for Eq. (15), second-order case, using different strength of penalty parameter Γ

N	$\Gamma = 1$	$q(1)$	$\Gamma = 1.2$	$q(1.2)$	$\Gamma = 5$	$q(5)$	Projection	$q(P)$
51	−1.28	0.00	−1.50	0.00	−1.52	0.00	0.06	0.00
101	−1.47	0.64	−2.12	2.09	−2.13	2.03	−0.24	1.02
201	−1.62	0.51	−2.72	2.02	−2.73	2.02	−0.54	1.01
301	−1.71	0.50	−3.08	2.03	−3.08	2.01	−0.72	1.01
401	−1.77	0.50	−3.33	2.01	−3.33	2.01	−0.84	1.01

Also comparing to the projection method.

Table 4
$\log(l_2 - \text{error})$ and convergence for Eq. (15), fourth-order case, using different strength of penalty parameter Γ

N	$\Gamma = 1$	$q(1)$	$\Gamma = 1.2$	$q(1.2)$	$\Gamma = 5$	$q(5)$	Projection	$q(P)$
51	−2.33	0.00	−3.22	0.00	−3.29	0.00	−1.37	0.00
101	−3.05	2.44	−4.48	4.22	−4.54	4.21	−2.25	2.97
201	−3.80	2.49	−5.75	4.24	−5.78	4.17	−3.15	3.01
301	−4.24	2.50	−6.48	4.16	−6.50	4.10	−3.68	3.01
401	−4.55	2.50	−6.99	4.11	−7.01	4.07	−4.05	3.01

Also comparing to the projection method.

4.1. High-order finite difference method in 1-D

The spectral radius of $h^2\ Q$ for the semi-discrete problem Eq. (15) as a function of the penalty strength Γ is presented in Table 2. We compare the second-, fourth- and the sixth-order accurate cases, and include the corresponding results using the

Table 5
$\log(l_2 - \text{error})$ and convergence for Eq. (15), sixth-order case, using different strength of penalty parameter Γ

N	$\Gamma = 1$	$q(1)$	$\Gamma = 1.2$	$q(1.2)$	$\Gamma = 5$	$q(5)$	Projection	$q(P)$
51	−2.38	0.00	−3.83	0.00	−4.11	0.00	−2.27	0.00
101	−3.70	4.45	−5.71	6.33	−6.10	6.69	−3.76	5.01
201	−5.05	4.50	−7.68	6.59	−8.05	6.55	−5.26	5.02
301	−5.84	4.51	−8.80	6.39	−9.17	6.38	−6.14	5.02
401	−6.40	4.51	−9.62	6.61	−10.01	6.70	−6.77	5.02

Also comparing to the projection method.

Table 6
$\log(l_2 - \text{error})$ and convergence using a second-order unstructured FV discretization in a discontinuous media

Δx	$\log(l_2)$	q
0.0625	−1.11	
0.03125	−1.70	1.97
0.015625	−2.31	2.07
0.0078125	−2.92	2.04
0.00390625	−3.52	2.00

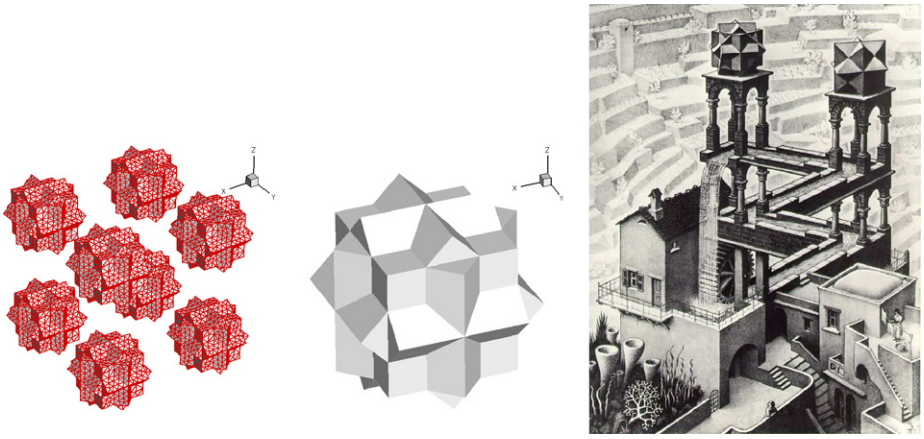

Fig. 2. Geometrical details and inspiration for the three cube compounds.

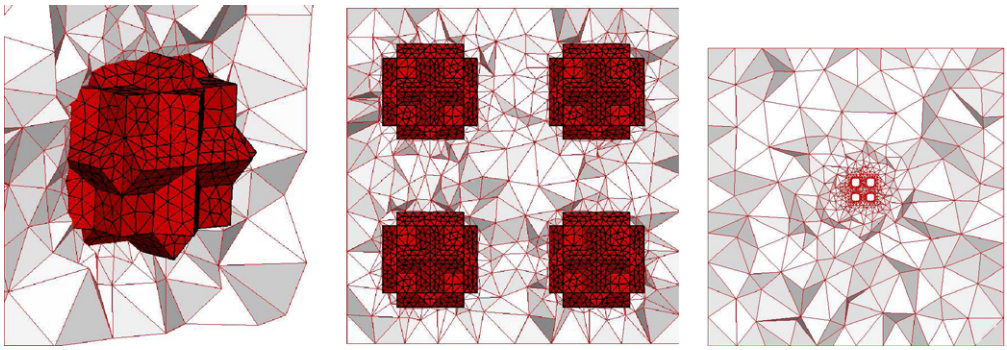

Fig. 3. Plane cut through coarse grid, different views (zoom).

projection method (see [24] for details). The stiffness increases with a larger Γ. The convergence results are shown in Tables 3–5 showing the improved accuracy with increased penalty strength Γ. A direct comparison with the projection method [24] is also presented. The simulation is run to $t = 1$ with a time-step small enough to make the time discretization error negligible (compared to the spatial discretization error). The SAT method is much more accurate (for $\Gamma > 1$) than the projection method, and leads to a higher convergence rate. The sixth-order case should in theory only lead to fifth-order convergence (see [32] for more information on the accuracy of finite difference approximations), but yields a result closer to seventh-order (see Table 5). (This is a remarkable result that needs further study since it contradicts the convergence analysis in [32].)

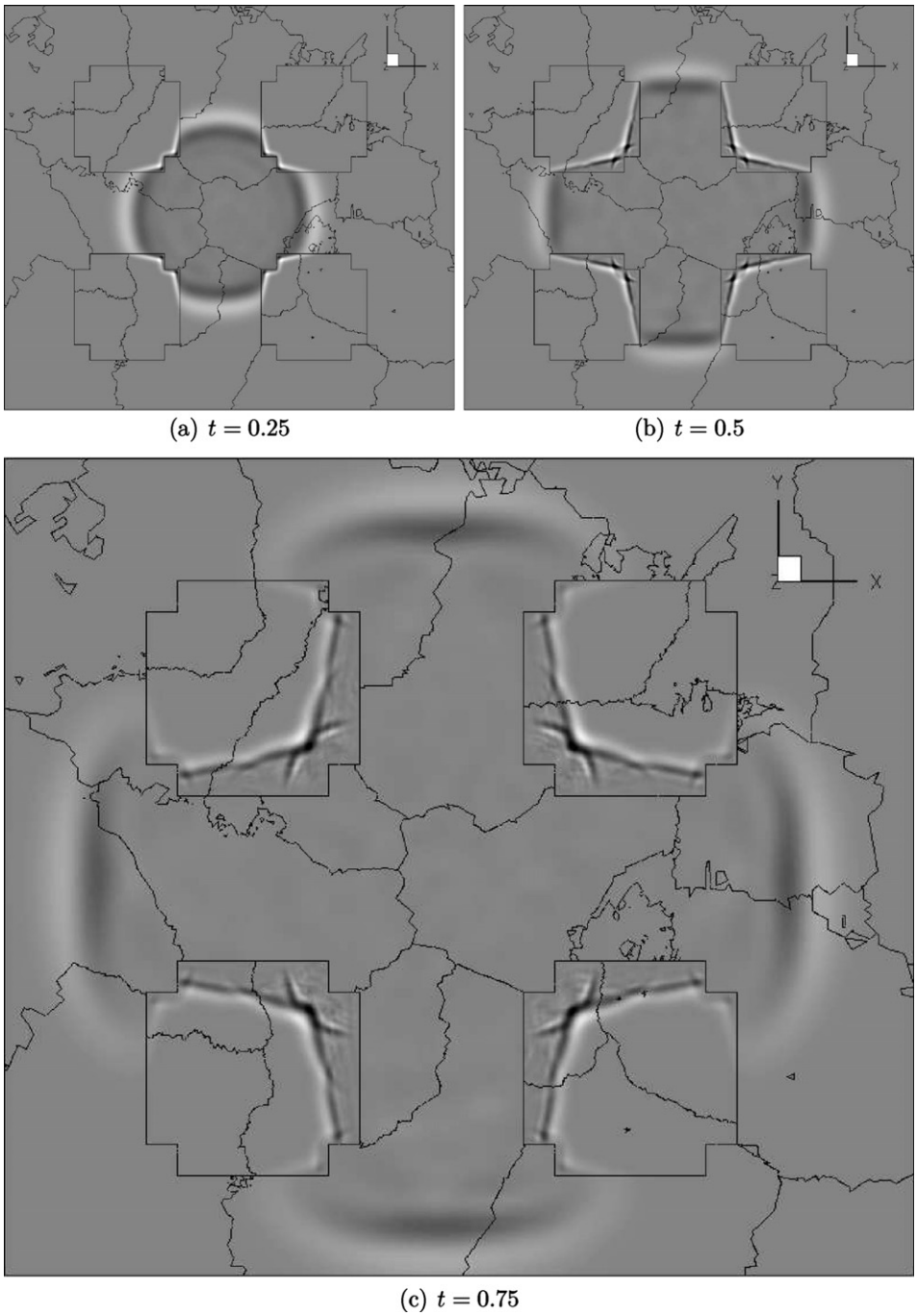

Fig. 4. Propagation of a 3-D Gaussian pulse on the $2 \times 2 \times 2$ array of 3-cube compounds with discontinuous interface.

The spectral radius of h^2Q is slightly larger for the SAT method compared to the projection method, depending on the value of Γ, see Table 2.

4.2. Finite volume method in 3-D

The present method has been implemented for unstructured tetrahedral grids in a discontinuous media, using the node-based SBP finite-volume discretization. In the first test we verify the accuracy of Eq. (20). We chose the analytic 1-D solution given by Eq. (21), and compute the solution on a cubic two-block domain. (As for the 1-D case we use $a_1 = b_1 = 1,\ a_2 = b_2 = 0.6$, $n = 1$ and $m = 2$.) A convergence study is shown in Table 6.

Finally, as a qualitative illustration of the method's capability, we compute the 3-D propagation of a Gaussian pulse in a volume surrounding a $2 \times 2 \times 2$ array of 3-cube compounds (see Fig. 2) made of a different material. We use $a_1 = b_1 = 1$ on the outside domain and $a_2 = b_2 = 0.2$ inside the cubes. Inspiration for this choice of geometry comes from M.C. Escher's Waterfall (see Fig. 2). Our cubes have a characteristic dimension of 0.2, and have center-to-center spacing of 0.5 in a $1 \times 1 \times 1$ box. The simulations reported below (see Fig. 4) were run on a grid produced by three applications of recursive tetrahedral refinement to the coarse grid shown in Fig. 3. The simulations were initiated with a stationary Gaussian pulse $\exp(-((x-x_c)^2 + (y-y_c)^2 + (z-z_c)^2)/0.03^2)$ in the plane of four of the polyhedra and offset slightly along the diagonal to break the fourfold symmetry.

The grid for this simulation consisted of 31,126,528 tetrahedra in the surrounding media and roughly the same inside the cubes. The time-step is $\Delta t = 0.00025$. Results are plotted on a plane passing through the center of four of the polyhedra for three times, $t = 0.25$, $t = 0.5$, and $t = 0.75$. The location of the center of the initial pulse is in this plane and displaced slightly toward the upper right, producing the observed diagonal asymmetry. The lines that can be seen in Fig. 4 illustrate the partitioning among the processors.

Remark. This simulation was done primarily to show that the present SBP–SAT technique can be utilized for large scale simulations using computational tools from the production code CDP. A grid convergence study for this problem was not performed, since it would be very costly to derive a reference solution. An assessment of the number of unknowns needed to resolve the wave-propagation was not done.

5. Conclusions and future work

We have proven that narrow-stencil approximations of the second-order acoustic wave equation in discontinuous media are time-stable, when combining narrow-diagonal SBP operators and the SAT penalty technique to impose the boundary and interface conditions. The accuracy and stability of the present method have been verified by numerical simulations in 1-D using high-order finite difference discretizations and in 3-D using the unstructured finite volume discretization utilized by the production code CDP. A direct comparison with the projection method was done in 1-D, with the conclusion that the newly constructed SAT method is very much favorable.

Future work will include the application of the present SBP–SAT technique to systems of second-order hyperbolic equations such as the elastic wave equations and Maxwell's equations. To further increase the efficiency of the method we will propose a hybrid discretization, by combining (using the SAT technique) the high-order accurate SBP discretizations and the unstructured SBP discretization discussed in the present study.

Appendix I. Narrow-diagonal second-derivative SBP operators

Proof of Lemma 2.3. The dissipative part M_b of a narrow-diagonal second-derivative SBP operator can be factorized like $M_b = S^{\mathrm{T}}RS$. Since M_b by construction is positive semi-definite, this also holds for R. The positive semi-definite matrix R is then split into

$$R = \widetilde{R} - h\ \mathrm{diag}(b_0\alpha, 0, \ldots, 0, b_N\alpha).$$

By using the symbolic mathematics program MAPLE we can numerically derive the limiting value of α, such that $\widetilde{R} = R - h\ \mathrm{diag}(b_0\alpha, 0, \ldots, 0, b_N\alpha)$ is positive semi-definite. The value of α depends on the numerical scheme and b, but is independent of the grid-size h, for a sufficiently resolved b. A properly chosen α means that $\widetilde{R}$ is positive semi-definite, which also holds for $\widetilde{M}_b = S^{\mathrm{T}}\widetilde{R}S$. By construction

$$v^{\mathrm{T}}M_b v = (Sv)^{\mathrm{T}}R(Sv) = h\ \frac{\alpha}{b_0}(BSv)_0^2 + h\ \frac{\alpha}{b_N}(BSv)_N^2 + v^{\mathrm{T}}\widetilde{M}_b v,$$

which show that (7) holds. □

We now present the specific forms of the narrow-diagonal SBP operators used in the analysis. We consider the second-, fourth- and sixth-order accurate discretizations.

I.1. The second-order case

The norm is defined by

$$H = h\begin{bmatrix} \frac{1}{2} & & & & \\ & 1 & & & \\ & & \ddots & & \\ & & & 1 & 0 \\ & & & & \frac{1}{2} \end{bmatrix}.$$

The narrow-diagonal second-derivative SBP operator for variable coefficients are given by

$$D_2 = H^{-1}(-D^{\mathrm{T}}\widetilde{B}\,D + BS),$$

where

$$D = \frac{1}{h}\begin{bmatrix} -1 & 1 & & & \\ & -1 & 1 & & \\ & & \ddots & & \\ & & & -1 & 1 \\ & & & -1 & 1 \end{bmatrix} \quad \widetilde{B} = \frac{h}{2}\begin{bmatrix} b_0 + b_1 & & & & \\ & b_1 + b_2 & & & \\ & & \ddots & & \\ & & & b_{N-1} + b_N & \\ & & & & 0 \end{bmatrix}$$

and

$$B = \begin{bmatrix} -b_0 & & & & \\ & 0 & & & \\ & & \ddots & & \\ & & & 0 & \\ & & & & b_N \end{bmatrix} \quad S = \frac{1}{h}\begin{bmatrix} -1 & 1 & & & \\ & 1 & & & \\ & & \ddots & & \\ & & & 1 & \\ & & & -1 & 1 \end{bmatrix}.$$

For the special case of constant b we obtain

$$D^{\mathrm{T}}\widetilde{B}\,D = M = \frac{1}{h}\begin{bmatrix} 1 & -1 & & & & & \\ -1 & 2 & -1 & & & & \\ & & & \ddots & & & \\ & & & & -1 & 2 & -1 \\ & & & & & -1 & 1 \end{bmatrix}.$$

In [24] we use a more accurate approximation of the boundary derivative, given by

$$S = \frac{1}{h}\begin{bmatrix} \frac{3}{2} & -2 & \frac{1}{2} & & & \\ & 1 & & & & \\ & & \ddots & & & \\ & & & 1 & & \\ & & & \frac{1}{2} & -2 & \frac{3}{2} \end{bmatrix},$$

which leads to $\alpha = 0.4$ (instead of 1, see Table 1).

I.2. The fourth-order case

The discrete norm is given by: $H = h\ \mathrm{diag}(\frac{17}{48}, \frac{59}{48}, \frac{43}{48}, \frac{49}{48}, 1, \ldots)$. The M and S operators (using 9 points) are given by

$$M=\frac{1}{h}\begin{bmatrix}
\frac{9}{8} & -\frac{59}{48} & \frac{1}{12} & \frac{1}{48} & & & & & & \\
-\frac{59}{48} & \frac{59}{24} & -\frac{59}{48} & & & & & & & \\
\frac{1}{12} & -\frac{59}{48} & \frac{55}{24} & -\frac{59}{48} & \frac{1}{12} & & & & & \\
\frac{1}{48} & 0 & -\frac{59}{48} & \frac{59}{24} & -\frac{4}{3} & \frac{1}{12} & & & & \\
 & & \frac{1}{12} & -\frac{4}{3} & \frac{5}{2} & -\frac{4}{3} & \frac{1}{12} & & & \\
 & & & & \ddots & & & & & \\
 & & \frac{1}{12} & -\frac{4}{3} & \frac{5}{2} & -\frac{4}{3} & \frac{1}{12} & & & \\
 & & & \frac{1}{12} & -\frac{4}{3} & \frac{59}{24} & -\frac{59}{48} & 0 & \frac{1}{48} & \\
 & & & & \frac{1}{12} & -\frac{59}{48} & \frac{55}{24} & -\frac{59}{48} & \frac{1}{12} & \\
 & & & & & & -\frac{59}{48} & \frac{59}{24} & -\frac{59}{48} & \\
 & & & & & \frac{1}{48} & \frac{1}{12} & -\frac{59}{48} & \frac{9}{8} &
\end{bmatrix},$$

$$S=\frac{1}{h}\begin{bmatrix}
\frac{11}{6} & -3 & \frac{3}{2} & -\frac{1}{3} & & & & \\
 & 1 & & & & & & \\
 & & & & & & & \\
 & & & \ddots & & & & \\
 & & & & & & & \\
 & & & & & 1 & & \\
 & & & & -\frac{1}{3} & \frac{3}{2} & -3 & \frac{11}{6}
\end{bmatrix}.$$

I.3. The sixth-order case

The discrete norm is given by: $H = h\ \mathrm{diag}(\frac{13649}{43200}, \frac{12013}{8640}, \frac{2711}{4320}, \frac{5359}{4320}, \frac{7877}{8640}, \frac{43801}{43200}, 1, \ldots)$. The 5th-order accurate boundary derivative operator is given by

$$S=\frac{1}{h}\begin{bmatrix}
-\frac{25}{12} & 4 & -3 & \frac{4}{3} & \frac{1}{4} & & \\
 & & 1 & & & & \\
 & & & & & & \\
 & & & \ddots & & & \\
 & & & & & & \\
 & & & & 1 & & \\
 & & \frac{1}{4} & -\frac{4}{3} & 3 & -4 & \frac{25}{12}
\end{bmatrix}.$$

The left boundary closure of hM is given by

$$\begin{aligned}
m_{1,1} &= \frac{15583}{12960} & m_{2,3} &= -\frac{134603}{51840} & m_{3,6} &= -\frac{30409}{86400} & m_{5,7} &= \frac{3}{20} \\
m_{1,2} &= -\frac{253093}{172800} & m_{2,4} &= \frac{4141}{2880} & m_{4,4} &= \frac{37967}{6480} & m_{5,8} &= -\frac{1}{90} \\
m_{1,3} &= \frac{52391}{129600} & m_{2,5} &= -\frac{86551}{103680} & m_{4,5} &= -\frac{53369}{17280} & m_{6,6} &= \frac{49}{18} \\
m_{1,4} &= -\frac{68603}{259200} & m_{2,6} &= \frac{24641}{129600} & m_{4,6} &= \frac{54899}{129600} & m_{6,7} &= -\frac{3}{2} \\
m_{1,5} &= \frac{2351}{14400} & m_{3,3} &= \frac{10991}{2160} & m_{4,7} &= -\frac{1}{90} & m_{6,8} &= \frac{3}{20} \\
m_{1,6} &= -\frac{4207}{103680} & m_{3,4} &= -\frac{22583}{5184} & m_{5,5} &= \frac{2747}{810} & m_{6,9} &= -\frac{1}{90} \\
m_{2,2} &= \frac{42353}{12960} & m_{3,5} &= \frac{46969}{25920} & m_{5,6} &= -\frac{820271}{518400}
\end{aligned}$$

In the interior we have the symmetric scheme: $-h\ (M\ v)_j = \frac{1}{90} v_{j-3} - \frac{3}{20}\ v_{j-2} + \frac{3}{2}\ v_{j-1} - \frac{49}{18}\ v_j + \frac{3}{2}\ v_{j+1} - \frac{3}{20}\ v_{j+2} + \frac{1}{90}\ v_{j+3}$.

References

[1] A. Bamberger, R. Glowinski, Q.H. Tran, A domain decomposition method for the acoustic wave equation with discontinuous coefficients and grid change, SIAM J. Numer. Anal. 34 (2) (1997) 603–639.

[2] A. Bayliss, K.E. Jordan, B.J. Lemesurier, E. Turkel, A fourth order accurate finite difference scheme for the computation of elastic waves, Bull. Seismol. Soc. Amer. 76 (4) (1986) 1115–1132.

[3] G. Calabrese, Finite differencing second order systems describing black holes, Phys. Rev. D 71 (2005) 027501.

[4] M.H. Carpenter, D. Gottlieb, S. Abarbanel, Time-stable boundary conditions for finite-difference schemes solving hyperbolic systems: methodology and application to high-order compact schemes, J. Comput. Phys. 111 (2) (1994).

[5] M.H. Carpenter, D. Gottlieb, S. Abarbanel, Time-stable boundary conditions for finite-difference schemes solving hyperbolic systems: methodology and application to high-order compact schemes, J. Comput. Phys. 111 (2) (1994).

[6] M.H. Carpenter, J. Nordström, D. Gottlieb, A stable and conservative interface treatment of arbitrary spatial accuracy, J. Comput. Phys. 148 (1999).

[7] G. Cohen, P. Joly, Construction and analysis of fourth-order finite difference schemes for the acoustic wave equation in nonhomogeneous media, SIAM J. Numer. Anal. 33 (4) (1996) 1266–1302.
[8] M. Grote, A. Schneebeli, D. Schötzau, Discontinuous Galerkin finite element method for the wave equation, SIAM J. Numer. Anal. 44 (2006) 2408–2431.
[9] M. Grote, A. Schneebeli, D. Schötzau, Interior penalty discontinuous Galerkin method for Maxwell's equations: energy norm error estimates, J. Comput. Appl. Math. 204 (2007) 375–386.
[10] B. Gustafsson, H.O. Kreiss, A. Sundström, Stability theory of difference approximations for mixed initial boundary value problems, Math. Comp. 26 (119) (1972).
[11] B. Gustafsson, E. Mossberg, Time compact high order difference methods for wave propagation, SIAM J. Sci. Comput. 26 (2004) 259–271.
[12] B. Gustafsson, P. Wahlund, Time compact difference methods for wave propagation in discontinuous media, SIAM J. Sci. Comput. 26 (2004) 272–293.
[13] T. Hagstrom, Radiation boundary conditions for the numerical simulation of waves, Acta Numer. (1999) 47–106.
[14] F. Ham, K. Mattsson, G. Iaccarino, P. Moin, Towards time-stable and accurate LES on unstructured grids, Lect. Notes Comput. Sci. Eng. 56 (2007) 235–250.
[15] K.R. Kelly, R.W. Ward, S. Treitel, R.M. Alford, Synthetic seismograms: a finite difference approach, Geophysics 41 (1976) 2–27.
[16] H.-O. Kreiss, N.A. Petersson, An embedded boundary method for the wave equation with discontinuous coefficients, SIAM J. Sci. Comput. 28 (2006) 2054–2074.
[17] H.-O. Kreiss, N.A. Petersson, A second order accurate embedded boundary method for the wave equation with dirichlet data, SIAM J. Sci. Comput. 27 (2006) 1141–1167.
[18] H.-O. Kreiss, N.A. Petersson, J. Yström, Difference approximations for the second order wave equation, SIAM J. Numer. Anal. 40 (2002) 1940–1967.
[19] H.-O. Kreiss, N.A. Petersson, J. Yström, Difference approximations of the Neumann problem for the second order wave equation, SIAM J. Numer. Anal. 42 (2004) 1292–1323.
[20] H.-O. Kreiss, G. Scherer, Finite element and finite difference methods for hyperbolic partial differential equations, Mathematical Aspects of Finite Elements in Partial Differential Equations, Academic Press, Inc., 1974.
[21] Heinz-Otto Kreiss, Joseph Oliger, Comparison of accurate methods for the integration of hyperbolic equations, Tellus XXIV (1972) 3.
[22] S.K. Lele, Compact finite difference schemes with spectral-like resolution, J. Comput. Phys. 103 (1992) 16–42.
[23] K. Mattsson, J. Nordström, Summation by parts operators for finite difference approximations of second derivatives, J. Comput. Phys. 199 (2) (2004) 503–540.
[24] K. Mattsson, J. Nordström, High order finite difference methods for wave propagation in discontinuous media, J. Comput. Phys. 220 (2006) 249–269.
[25] K. Mattsson, M. Svärd, M. Shoeybi, Stable and accurate schemes for the compressible Navier–Stokes equations, J. Comput. Phys. 227 (4) (2008) 2293–2316.
[26] J. Nordström, K. Mattsson, R.C. Swanson, Boundary conditions for a divergence free velocity–pressure formulation of the incompressible Navier–Stokes equations, J. Comput. Phys. 225 (2007) 874–890.
[27] J. Nycander, Tidal generation of internal waves from a periodic array of steep ridges, J. Fluid Mech. 567 (2006) 415–432.
[28] P. Olsson, Summation by parts, projections, and stability I, Math. Comp. 64 (1995) 1035.
[29] P. Olsson, Summation by parts, projections, and stability II, Math. Comp. 64 (1995) 1473.
[30] G.R. Shubin, J.B. Bell, A modified equation approach to constructing fourth order methods for acoustic wave propagation, SIAM J. Sci. Stat. Comput. 8 (2) (1987) 135–151.
[31] B. Strand, Summation by parts for finite difference approximations for d/d*x*, J. Comput. Phys. 110 (1994) 47–67.
[32] M. Svärd, J. Nordström, On the order of accuracy for difference approximations of initial-boundary value problems, J. Comput. Phys. 218 (October) (2006) 333–352.
[33] B. Szilagyl, H.-O. Kreiss, J.W. Winicour, Modeling the black hole excision problem, Phys. Rev. D 71 (2005) 104035.
[34] S.V. Tsynkov, Numerical solution of problems on unbounded domains. a review, Appl. Numer. Math. (1998) 465–532.
[35] J. Virieux, Sh-wave propagation in heterogeneous media: velocity–stress finite-difference method, Geophysics 49 (1984) 1933–1957.
[36] J. Virieux, P-sv wave propagation in heterogeneous media: velocity–stress finite-difference method, Geophysics 51 (1986) 889–901.
[37] K.S. Yee, Numerical solution of initial boundary value problems involving Maxwell's equations in isotropic media, IEEE Trans. Antennas Propag. 14 (1966) 302–307.